

Original Article

NiCdFe₂O₄ Spinel ferrite: Novel synthesis, insights into the antibacterial mechanism and potential cytotoxic effect

Salhah Hamed Alrefaee*

^aDepartment of Chemistry, College of Science, Taibah University, Yanbu Governorate, Saudi Arabia

ARTICLE INFO

Keywords:

Antibacterial
Co-precipitate
Cytotoxicity
Magnetic nanoparticles
Spinel ferrite

ABSTRACT

This study synthesized NiCdFe₂O₄ for medical applications using a co-precipitate method. The nanoparticles were examined by high-resolution transmission electron microscopy (HR-TEM), X-ray diffraction (XRD), stability via zeta potential, UV, and Fourier transform infrared (FTIR) analysis. Polycrystalline and elemental identification and optical characteristics were used to investigate the geometry and architecture phase of the nanocomposite. The NiCdFe₂O₄ nanocomposite was found to be spherical with a crystallite size of less than 2 nm. The structural and magnetic properties were examined using FTIR and X-ray Diffraction. The nanoparticles demonstrated strong quantum confinement effects and superparamagnetic behavior at room temperature. The study tested NiCdFe₂O₄ nanoparticles against six multidrug-resistant and two American type culture collection (ATCC) bacterial strains, with *K. pneumoniae* being the most resistant. The nanoparticles effectively trapped bacterial infections by binding to areas on the *K. pneumoniae* surface, damaging the membrane's structural integrity. The efficiency of capture increased dramatically when the infection duration was increased from 40 to 120 min.

1. Introduction

Bacterial infections continue to pose a severe threat to global health, with antibiotic resistance making treatment increasingly difficult. The World Health Organization [1] reports that drug-resistant bacteria cause over 1.27 million deaths each year, a number that could rise without new treatment strategies. Traditional antibiotics, once highly effective, are now struggling against resistant strains like multidrug-resistant *Staphylococcus aureus* (MRSA) and *Klebsiella pneumoniae* [2]. One promising solution lies in magnetic nanoparticles (MNPs), particularly spinel ferrites such as NiCdFe₂O₄ and Fe₃O₄, which can deliver drugs more precisely, generate reactive oxygen species (ROS), and physically damage bacterial cell walls [3].

In recent years, nanocomposite materials have revolutionized medicine due to their high efficiency, targeted delivery, and ability to bypass bacterial resistance mechanisms [4]. Among these, magnetic spinel ferrites (MFe₂O₄) stand out because of their stability, strong magnetic properties, and proven antibacterial effects [5]. These nanoparticles can be synthesized using various methods, including the sol-gel, hydrothermal, and co-precipitation methods. The activity of this catalyst in organic transformations comes from its combination of Brønsted and Lewis acid sites, engineered through a co-precipitation method. By carrying out the precipitation under hydrothermal conditions, we can carefully manage the reaction to produce a nanocatalyst with a small, uniform particle size and controlled morphology, a key reason for its current appeal in research. The co-precipitation method is particularly suitable for producing NiCdFe₂O₄ nanoparticles due to its simplicity, cost-effectiveness, and low-temperature operation [6].

However, it has some drawbacks, such as particle agglomeration and inconsistent crystallinity, which can be improved by adjusting reaction conditions [7].

Studies comparing Fe₃O₄ nanoparticles to conventional antibiotics have shown that nanoparticles often outperform traditional drugs, particularly against bacteria that are resistant to antibiotics. For example, Fe₃O₄ nanoparticles have demonstrated strong antibacterial activity against *E. coli* and *S. aureus* by disrupting cell membranes and inducing oxidative stress [8]. In contrast, many antibiotics fail against resistant strains because bacteria can break them down enzymatically [9]. Additionally, nanoparticles can be coated with antibiotics or natural antimicrobials (like chitosan), further enhancing their effectiveness [10].

As antibiotic resistance continues to grow, magnetic nanoparticles and nanocomposites offer a promising alternative, combining precision, reduced side effects, and the ability to overcome resistance [11]. Moving forward, these advanced materials could play a crucial role in ensuring that we stay ahead in the ongoing battle against bacterial infections.

While spinel ferrite nanoparticles have shown promising antibacterial properties, there remains a significant gap in research regarding NiCdFe₂O₄ nanocomposites synthesized via co-precipitation and their effects on bacterial pathogens. Our study addresses this by first developing this novel nanocomposite through co-precipitation, then thoroughly characterizing its structural and chemical properties using high-resolution-transmission electron microscopy (HR-TEM), X-ray diffraction (XRD), Fourier transform infrared (FTIR), energy-dispersive X-ray (EDX), UV-Vis spectroscopy, and zeta potential analysis. Building on this foundation, we then evaluate the material's antibacterial efficacy against standard ATCC bacterial strains, with

*Corresponding author:

E-mail address: Srfaay@taibahu.edu.sa (S. Elrefaee)

Received: 25 August, 2025 Accepted: 01 November, 2025 Epub Ahead of Print: 23 February, 2026 Published: 02 May, 2026

DOI: 10.25259/AJC_1019_2025

This is an open-access article distributed under the terms of the Creative Commons Attribution-Non Commercial-Share Alike 4.0 License, which allows others to remix, transform, and build upon the work non-commercially, as long as the author is credited and the new creations are licensed under the identical terms.

particular focus on understanding its mechanism of action, whether through reactive oxygen species generation, physical disruption of cell membranes, or other inhibitory pathways. This two-pronged approach not only introduces a new antibacterial nanomaterial to the scientific community but also provides crucial insights into its potential biomedical applications.

2. Materials and Methods

2.1. Nano preparation

$\text{Ni}_{0.9}\text{Cd}_{0.1}\text{Fe}_2\text{O}_4$ was prepared by using a modified citrate-gel coprecipitation technique, individual aqueous solutions. The first solution was prepared by dissolving metal nitrate precursors in distilled water. To synthesize the $\text{Ni}_{0.9}\text{Cd}_{0.1}\text{Fe}_2\text{O}_4$ nanocomposite, precise stoichiometric amounts of 2.6165 g of $\text{Ni}(\text{NO}_3)_2 \cdot 6\text{H}_2\text{O}$, 0.3084 g of $\text{Cd}(\text{NO}_3)_2 \cdot 4\text{H}_2\text{O}$, and 8.0800 g of $\text{Fe}(\text{NO}_3)_3 \cdot 9\text{H}_2\text{O}$ were used. The second solution contained 9.4614 g of citric acid ($\text{C}_6\text{H}_8\text{O}_7$) as the complexing agent, dissolved in distilled water.

The metal nitrate and citric acid solutions were then combined in a 1:3 molar ratio and continuously stirred at 80°C (550 rpm) to form a homogeneous mixture. By carefully adding sodium hydroxide as a precipitating agent, the pH was adjusted to approximately 9, maintaining these conditions for 3 h until a characteristic dark brown precipitate formed. The product was filtered through multiple washing cycles with deionized water and acetone before oven-drying at 100°C. Finally, the samples were annealed at a temperature of 600°C for 3 h in a muffle furnace to optimize the crystalline structure. The resulting powder was collected and subjected to a final calcination process at 600°C for 3 h in a muffle furnace to obtain the crystalline $\text{Ni}_{0.9}\text{Cd}_{0.1}\text{Fe}_2\text{O}_4$ nanocomposite to obtain fine and controlled narrow particle size distribution (Figure 1).

2.2. Antibacterial activity

Antimicrobial activity is assessed using a disc diffusion test [12]. 100 $\mu\text{g} \cdot \text{mL}^{-1}$ of the tested pathogens' fresh overnight cultures were put onto nutrient-rich agar and allowed them to harden for 15 to 20 min. The sterile discs measuring 7-8 mm were used. Various concentrations of $\text{NiCdFe}_2\text{O}_4$ nanocomposites (50, 100, and 150 $\mu\text{g} \cdot \text{mL}^{-1}$) were applied to each disc. To encourage microbial development, the plates were incubated at 37°C for 24 h after letting the nanoparticles sink into the discs for 30 min at room temperature [13]. Triplicates of each experiment were conducted. To compare potential inhibition, Cefoxitin (1 $\text{mg} \cdot \text{mL}^{-1}$) was examined. The results were expressed as the widths of the inhibitory zones around the discs filled with $\text{NiCdFe}_2\text{O}_4$ nanocomposites.

2.2.1. Reactive oxygen species (ROS) assay

The ROS generation assay was measured by using 2,7-dichlorofluorescein diacetate (DCFH-DA) dye to compare the extracellular ROS of the bacterial cells before and after treatment with the synthesized nanoparticles [14]. In which 5 mL of cell pellet was incubated for 30 min at 37°C in the dark with 100 μM DCFH-DA. A spectrofluorometer with excitation and emission wavelengths of 485 and 530 nm, respectively, was used to measure the resulting fluorescence.

2.2.2. Capturing of bacteria by the prepared magnetic nanoparticles

The most resistant organism was used to test the bacterial pathogen-capturing capabilities of $\text{NiCdFe}_2\text{O}_4$ nanocomposites. The infectious agent was allowed to defrost on ice for fifteen minutes before being placed on agar. Following a 16-h incubation period in a conventional cell culture setting (5% CO_2 , 37°C), the plate was allowed to dry. Centrifuge tubes were filled with 5 mL of Luria Broth (LB), and a single colony was inoculated into them. For the next 12 h, the bacteria in the centrifuge tubes were placed in a cell culture medium and mixed with agitation at 250 rpm. To achieve an optical density of 0.1 at 600 nm

(OD600) as determined by UV-vis spectroscopy, the bacterial solution was then diluted with Lysogeny broth (LB).

While keeping the volume of the solution at 6 mL, the following concentrations of $\text{NiCdFe}_2\text{O}_4$ nanocomposites dispersed in Phosphate buffer saline (PBS) were added to the tube holding the bacterial solution: 0.05, 0.5, 1.0, and 2.0 $\text{mg} \cdot \text{mL}^{-1}$. The control group received a bacterial culture without nanocomposites. As a particle control, tubes containing just LB were additionally supplemented with the nanoadsorbent suspensions at the same concentration as described above. The solutions were incubated in a rotary shaker set at 250 rpm for 18 h, and then magnetic separation was performed using an external magnet. The optical density (OD600) was measured using the supernatant. The remaining bacterial concentration at a maximum wavelength of $\lambda_{\text{max}} = 260$ nm was used to determine the effectiveness of bacterial capture by nanoadsorbents. According to Darabdhara *et al.* [15], the concentration of residual bacteria after adsorption by using the bacterium's standard calibration curve was calculated.

Intracellular leakage was evaluated by monitoring the impact of $\text{NiCdFe}_2\text{O}_4$ on total sugars and proteins as markers of bacterial membrane damage over time intervals from 0 to 48 hrs. Bacterial cells were exposed to twice the MIC of the synthesized $\text{NiCdFe}_2\text{O}_4$, and at chosen time points, the cultures were centrifuged at 15,000 rpm. The supernatant was then assayed for total sugars and proteins using the methods of Dubois *et al.* [16] and Bradford [17], respectively.

2.3. Cytotoxic effect

A cell line called Vero was obtained from the American Type Culture Collection (ATCC, Rockville, MD), which is derived from the African Green Monkey Kidney cell line. Moreover, the Human lung fibroblast (WI-38 cells) normal cell line (ATCC® number: CCL-75™) was obtained from the American Type Culture Collection (ATCC, Rockville, MD) and tested for the possible cytotoxic effect. Sigma (St. Louis, MO, USA) is the supplier for the chemicals used, which include dimethyl sulfoxide (DMSO), MTT, and trypan blue dye. Lonza (Belgium) was consulted for the acquisition of fetal bovine serum, DMEM, HEPES buffer solution, L-glutamine, gentamicin, and 0.25% Trypsin-EDTA.

2.3.1. Propagation of cell lines

Cells were cultured in Dulbecco's modified Eagle's medium (DMEM) with 10% heat-inactivated fetal bovine serum, 1% L-glutamine, HEPES buffer, and 50 $\mu\text{g}/\text{mL}$ gentamycin. Cells were maintained at 37°C in a humidified atmosphere containing 5% CO_2 and subcultured biweekly.

2.3.2. Assessment of cytotoxicity through viability assay

For the cytotoxicity test, 1×10^4 cells/well in 100 μL of growth media were planted onto a 96-well plate. A fresh medium containing $\text{NiCdFe}_2\text{O}_4$ nanoparticles of varied concentrations was added after 24 h of seeding. A 96-well plate was used to apply serial two-fold dilutions of the chemical component under test to confluent cell monolayers. For 24 h, the microtiter plates were placed in an incubator with 5% CO_2 and a humidifier set to 37°C. We used three wells to test the different concentrations of $\text{NiCdFe}_2\text{O}_4$. After incubation, a colorimetric assay was used to determine the cell viability yield. After incubating for 24 h, the MTT test was used to determine the number of viable cells. After removing the media from the 96-well plates, 100 μL of new medium was added. Then, all the wells, including the ones without treatment, were supplemented with 10 μL of the 12 mM MTT stock solution, which consisted of 5 mg of MTT in 1 mL of PBS. For 4 h, the 96-well plates were placed in an incubator set at 37°C with 5% CO_2 . After removing 85 μL of the medium from the wells, 50 μL of DMSO was added to every well. A pipette was used to mix the ingredients, and then they were incubated at 37°C for 10 min. For determining the quantity of viable cells, a microplate reader (SunRise, TECAN, Inc., USA) was used to measure the optical density at 590 nm. The percentage of viability was then computed as $[(\text{ODt}/\text{ODc})] \sim 100\%$. According to Abdel Ghany *et al.* [18] and Beal *et al.* [19], the mean optical density of untreated cells is denoted as ODc, whereas the mean optical density of wells that were exposed to the tested sample is denoted as ODt. Following treatment

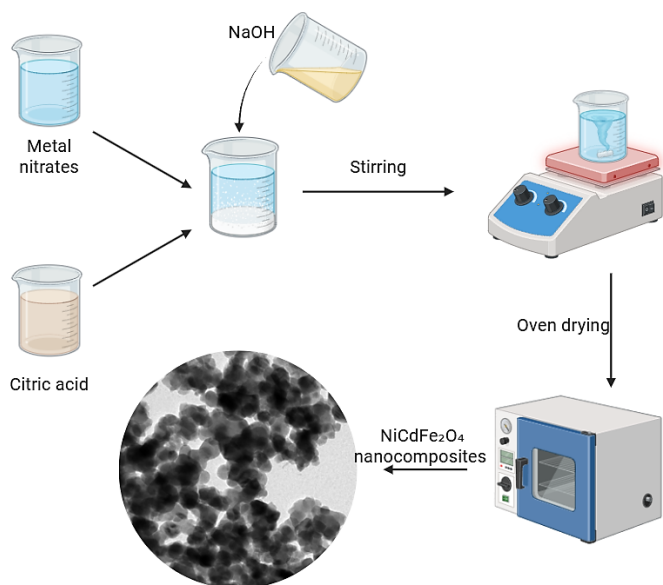


Figure 1. Sketch of the co-precipitation method.

with the specified chemical, the survival curve for each tumor cell line is obtained by illustrating the link between surviving cells and $\text{NiCdFe}_2\text{O}_4$. Graphpad Prism software (San Diego, CA, USA) was used to generate dose-response curves for each concentration. From these, the cytotoxic concentration (CC_{50}), which is defined as the dosage required to elicit toxic effects in 50% of intact cells, was computed.

2.4. Statistical analysis

The values' means \pm standard deviations (SD) were used to depict all data points. The statistical analysis was conducted using Origin 8.0 software. The data were subjected to analysis using one-way analysis of variance (ANOVA) in conjunction with Tukey's test to ascertain any disparities. The degrees of statistical significance were expressed as $*p < 0.05$ and $**p < 0.01$.

3. Results and Discussion

3.1. Characterization

HR-TEM was performed on nano-prepared samples to examine the morphology and confirm the nano-spherical shape of the sample with a range not exceeding 25 nm for magnetic nanoparticles. Fe dark spherical particle connected with a light hexagonal nickel and a light spherical particle, as appears in Figures 2(a, b). The size distribution was made using ImageJ software to determine the average particle diameter.

Figure 2(c) shows the XRD patterns of the $\text{NiCdFe}_2\text{O}_4$ powder synthesized using Co-precipitate. The XRD peaks corresponding to the cubic spinel ferrite phase structure are visible in the (220), (311), (222), (400), (422), (511), and (440) reflection planes corresponds to $2\theta = 30.8^\circ$ ($d = 2.88 \text{ \AA}$), 35.72° ($d = 2.548 \text{ \AA}$), 43.58° ($d = 2.389 \text{ \AA}$), 53.42° ($d = 1.823 \text{ \AA}$), 57.62° ($d = 1.756 \text{ \AA}$), 62.96° ($d = 1.523 \text{ \AA}$). These observed peaks closely match the expected diffraction pattern based on the reference file JCPDS 790416. The well-matched diffraction pattern, characterized by the high intensity of the reflected planes, serves as an indication of the high crystallinity of the synthesized powders. The XRD analysis confirms the successful formation of a single-phase spinel structure with the Fd3m space group. No additional phases originating

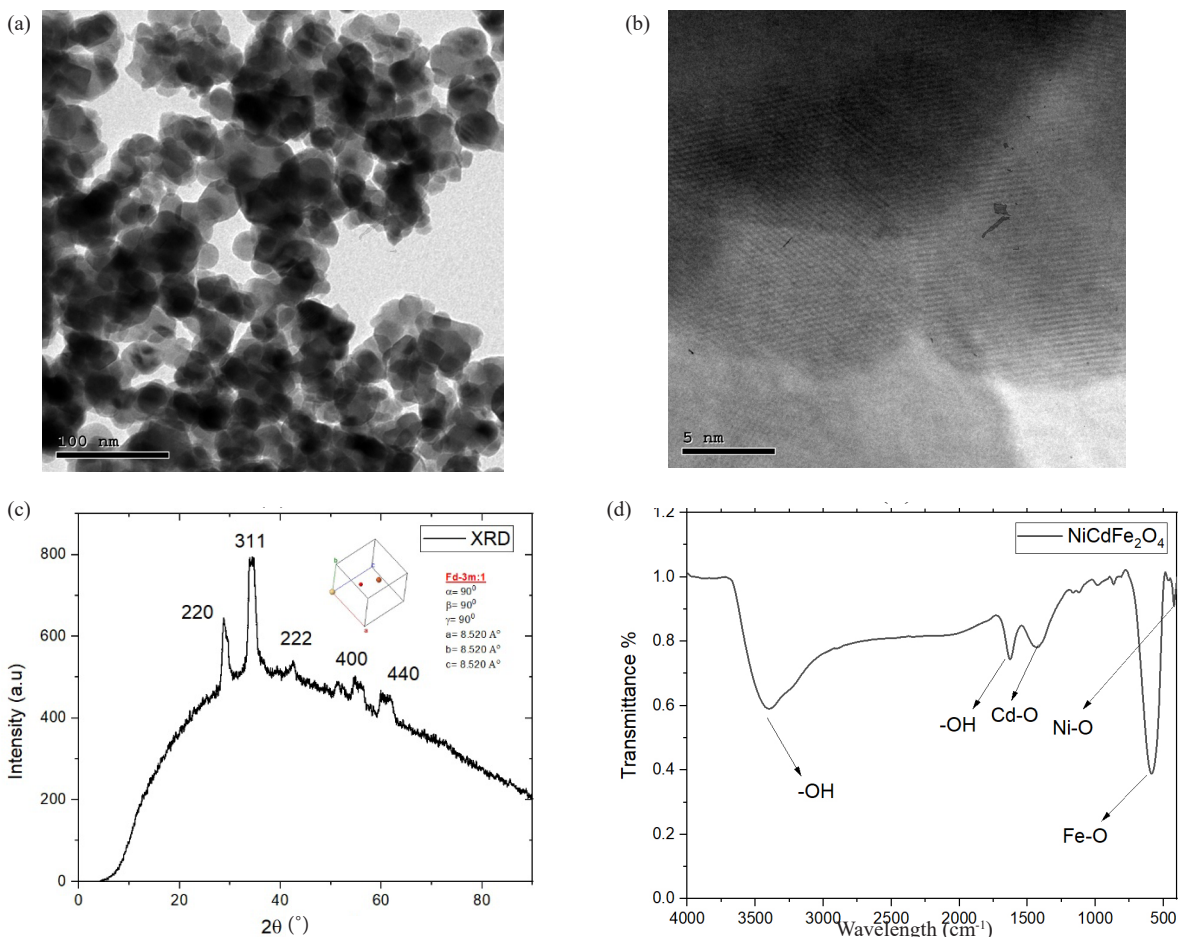


Figure 2. (a) TEM, (b) HR-TEM at 5 nm scale, (c) XRD, (d) FTIR analyses of $\text{NiCdFe}_2\text{O}_4$ nanocomposites.

from the starting materials or other contaminants were detected in the synthesized NiCdFe₂O₄ powders. This indicates that the synthesis process yielded a highly pure and phase-pure product [20]. The Debye-Scherrer equation [21] was used to compute the average crystallite size $D \approx 15$ nm as follows (Eq. 1):

$$D = \frac{\alpha\lambda}{\beta \cos\theta} \quad (1)$$

In Figure 2(d), the FTIR spectrum was studied from 500 to 4000 cm⁻¹, exhibiting significant vibrational peaks that indicate the composition of the Magnetic nanoparticles NiCdFe₂O₄ NPs. According to the literature, the peaks recorded in 3425-3450 cm⁻¹ are due to O-H stretching [22], the appearance of characteristic peaks at 1400 cm⁻¹ of Cd-O bond confirmed by previous literature [23], and the two absorption bands in the 600–400 cm⁻¹ wavenumber range. Two prominent absorption bands are found in the IR spectra. The absorption band observed at 586 cm⁻¹ and the band observed at 423 cm⁻¹ show the stretching of tetrahedral Fe-O and octahedral Ni-O, respectively [24], which ensures the formation of Cd-substituted NiFe₂O₄ NPs.

3.2. Antibacterial activity

The prepared nanoparticles were tested against six multidrug-resistant strains and two ATCC bacterial strains representing the most commonly isolated nosocomial strains. Data in Table 1 revealed that the inhibition zone (IZ) diameter and minimum inhibitory concentration (MIC) ranged from 15.0-23.0 mm and 50.0-100.0 µg·mL⁻¹, while the most resistant strain was *K. pneumoniae*; hence, it was chosen for further studies. Different concentrations of NiCdFe₂O₄ nanocomposites were prepared and tested for the potential antibacterial activity against the *K. pneumoniae* strain. Data showed that the ROS activity is concentration-dependent (Figure 3). When the concentration of nanoparticles was

Table 1. Antimicrobial activity of the prepared nanoparticles against multidrug-resistant strains.

Bacterial strains	Cefoxitin		NiCdFe ₂ O ₄ nanocomposites	
	IZ diameter (mm)	MIC (µg·mL ⁻¹)	IZ diameter (mm)	MIC (µg·mL ⁻¹)
<i>K. pneumoniae</i> ATCC	25.0 ± 0.0	50.0	20.0 ± 0.3	50.0
<i>S. aureus</i> ATCC	20.0 ± 1.0	50.0	23.0 ± 0.2	50.0
<i>K. pneumoniae</i>	17.0 ± 0.5	75.0	15.0 ± 0.2	100.0
<i>P. mirabilis</i>	20.0 ± 0.0	50.0	16.0 ± 0.5	100.0
<i>S. aureus</i>	23.0 ± 1.8	50.0	21.0 ± 0.7	50.0
MRSA	19.0 ± 0.0	75.0	16.0 ± 0.2	100.0
<i>E. coli</i>	16.0 ± 0.2	75.0	15.0 ± 0.8	100.0
<i>E. faecalis</i>	21.0 ± 0.0	50.0	19.0 ± 0.1	75.0

raised from 0.25 mg·mL⁻¹ to 1.5 mg·mL⁻¹, it was noticed that the quantity of reactive oxygen species rose by about 20% (Figure 3). Nanoparticles were found to have been adsorbed or incorporated onto the membrane of the treated bacterial cells of MNP-treated *K. pneumoniae* (Figure 4). Further TEM investigation of *K. pneumoniae* (control) (Figure 4a) and MNP-treated *K. pneumoniae* showed that NiCdFe₂O₄ nanocomposites effectively trap bacterial infections (particles bind to areas on the *K. pneumoniae* surface rather than the whole surface), as seen in Figure 4(b). The control bacteria, which were not exposed to magnetic nanoparticles, had unharmed cell walls, in contrast to the bacteria that were trapped by them. In addition, NiCdFe₂O₄ nanocomposites damage the structural integrity of the membrane by penetrating the lipid bilayer component, either partly or entirely. It seems that when NiCdFe₂O₄ nanocomposites come into contact with bacteria, they depolarize the membrane, which ultimately results in cell death. This interaction may involve the polar heads of membrane lipids and proteins (Figures 5a-d). Lee *et al.* [25] showed that zero-valent iron nanoparticles, with diameters varying from 10 to 80 nm, were able to penetrate *E. coli* membranes and render the bacteria inactive. Because of their strong interaction with bacterial membranes, metallic cobalt-based nanoparticles and poly(hexamethylene biguanide) modified magnetite kill *Escherichia coli* (Gram-negative) bacteria upon contact, as demonstrated by Bromberg *et al.* [26]. Gu *et al.* [27] found that Gram-negative bacteria may bind to vancomycin functionalized magnetic (FePt) nanoparticles due to flaws in their outer membrane. Reducing separation time was the primary benefit of employing additional MNPs for capture. It should be noted that after collecting harmful bacterial pathogens, wastewater in all samples did not include any remaining adsorbents (Fe₃O₄). This is yet another crucial feature of methods that use magnetic separation [13]. In the present work, Figure 5(a) displays the effectiveness of the prepared NiCdFe₂O₄ nanocomposites in capturing *K. pneumoniae* after an 18-h inoculation. Researchers have shown that the concentration of surface-designed magnetic nanoparticles has a significant impact on the efficacy of bacterial pathogen capture. In addition, as shown in Figure 5(b), the efficiency of capture rises dramatically when the inoculation duration is increased from 40 to 120 min. These findings are consistent with previous publications on the concentration- and time-dependent suppression of bacteria by nanoparticles [28] and show that NiCdFe₂O₄ had outstanding capture capability for *K. pneumoniae*. At 60 min, the bacteria had reached an adsorption equilibrium onto the Fe₃O₄ NPs. At pH 5, the adsorption efficiency was 93.67%, while at 25°C, it was 98.65% for Fe₃O₄B. The results show that the Fe₃O₄ NPs produced by the chemical co-precipitation method are more effective in adsorbing bacteria than those produced by the ball milling method. It is observed that at the chosen pH, the surface charge of Fe₃O₄B is greater than that of Fe₃O₄A. Therefore, it is projected that the electrostatic contact between the bacterial surface and the NP surface is greater in Fe₃O₄B than in Fe₃O₄A. Different concentrations of 0.1 g·L⁻¹, 0.2 g·L⁻¹, 0.3 g·L⁻¹, and 0.4 g·L⁻¹ of *E. coli* were taken into consideration. With an

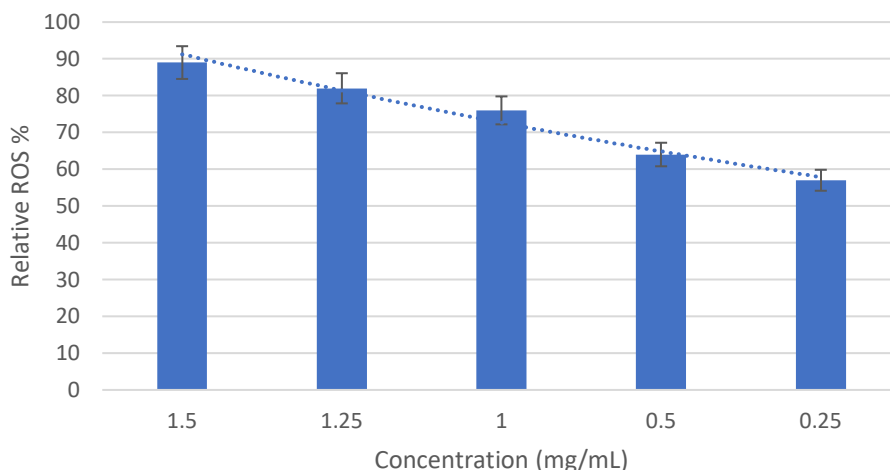


Figure 3. ROS activity of the prepared nanocomposite.

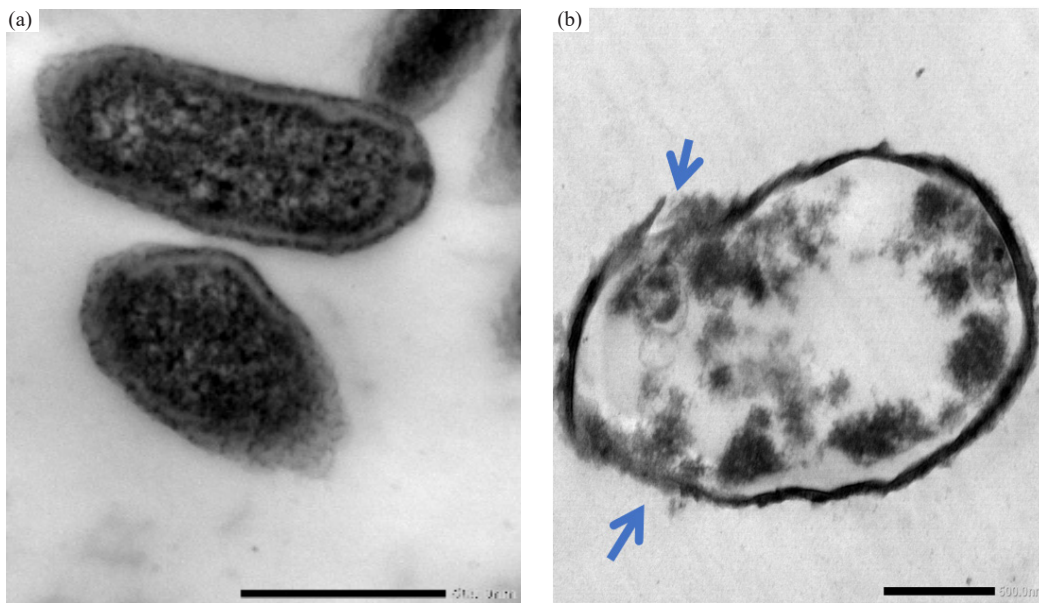


Figure 4. TEM micrographs of (a) *K. pneumoniae* control untreated cells and (b) *K. pneumoniae* after 18 h of incubation (blue arrows show the deformations in the bacterial cell wall).

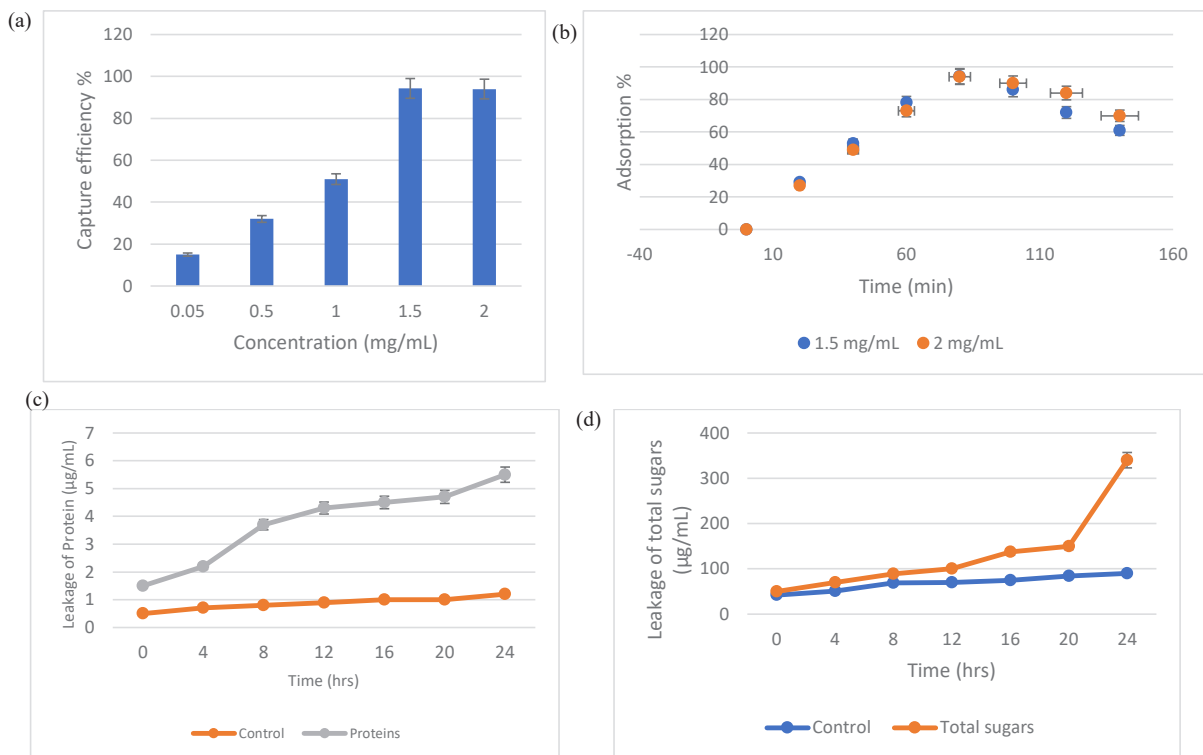


Figure 5. (a) Capture efficiency percentage, (b) Adsorption percentage, (c) Leakage of proteins, (d) and total sugars against *K. pneumoniae*-treated cells.

adsorbent concentration of $0.1 \text{ g}\cdot\text{L}^{-1}$, the greatest adsorption efficiency was seen. The adsorption effectiveness of the adsorbent reduced as the concentration of *E. coli* increased (more examples are presented in Table 3) [29-35]. Therefore, we thought that $0.1 \text{ g}\cdot\text{L}^{-1}$ was the optimal adsorbate concentration for future experiments.

3.3. Cytotoxic effect

The Cytotoxic activities against mammalian cells from African Green Monkey Kidney (Vero) and Human lung fibroblast (WI-38) cells were detected using MTT assay under these experimental conditions, with 50% cell cytotoxic concentration (CC_{50}) equal to 246.88 ± 4.94 and 260

$\pm 2.0 \text{ }\mu\text{g}\cdot\text{mL}^{-1}$, respectively (Figure 6, Table 2). At higher concentrations ($1000, 500, 250 \text{ }\mu\text{g}\cdot\text{mL}^{-1}$), there is substantial inhibition in VERO cells ($92.44\%, 73.11\%, 50.95\%$) but markedly lower inhibition in WI-38 cells ($90.2\%, 68.0\%, 39.31\%$), suggesting a differential cytotoxicity between the two cell lines. At moderate concentrations ($125 \text{ }\mu\text{g}\cdot\text{mL}^{-1}$ and below), VERO cells show detectable inhibition (12.88% at $125 \text{ }\mu\text{g}\cdot\text{mL}^{-1}$ and decreasing to near 0% as the concentration drops further), while WI-38 cells show very low or zero inhibition across $125 \text{ }\mu\text{g}\cdot\text{mL}^{-1}$ and below, with 0% observed from $62.5 \text{ }\mu\text{g}\cdot\text{mL}^{-1}$ downward.

$\text{NiCdFe}_2\text{O}_4$ nanocomposites exhibit appreciable antibacterial activity against multidrug-resistant strains (MICs $50\text{--}100 \text{ }\mu\text{g}\cdot\text{mL}^{-1}$, Table 1), consistent with a concentration-dependent effect suggested

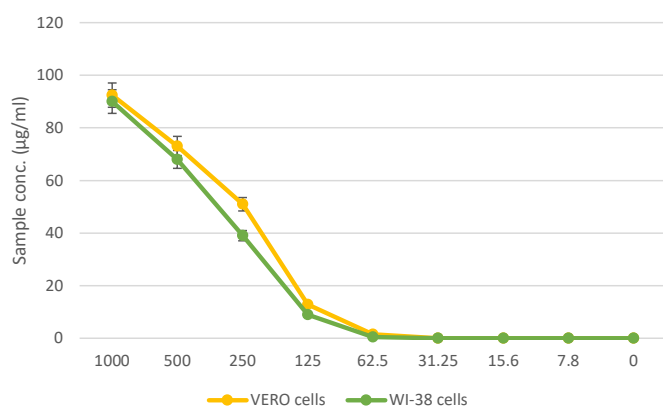


Figure 6. Cell viability graph of VERO and WI-38 cells after treatment with the prepared nanoparticles.

Table 2. Cell inhibitory effect of the prepared nanoparticles.

Sample conc. (µg·mL ⁻¹)	VERO cells	WI-38 cells
	Inhibitory % ± S.D.	Inhibitory % ± S.D.
1000	92.44 ± 0.82	90.2 ± 1.0
500	73.11 ± 1.33	68.0 ± 0.9
250	50.95 ± 1.59	39.31 ± 1.5
125	12.88 ± 1.41	9.6 ± 0.8
62.5	1.56 ± 0.72	0.5 ± 0.2
31.25	0	0
15.6	0	0
7.8	0	0
0	0	0

Table 3. Comparison of ferrite nanoparticles activity.

Nanoparticles	Activity	Reference
Silver-doped cobalt ferrite nanoparticles	Strongest antibacterial activity against both Gram-positive and Gram-negative strains, and can be easily removed from water with a magnetic field, reducing environmental contamination.	[29]
Zinc-coated cobalt ferrite nanoparticles	The antimicrobial activity was tested against <i>Salmonella typhi</i> and <i>Staphylococcus aureus</i> for both pure cobalt ferrite and zinc-doped cobalt ferrite nanoparticles, with Gram-negative strains showing a larger inhibition zone (22 mm) than pure cobalt ferrite (16 mm).	[30]
CoFe ₂ O ₄ nanoparticles	CoFe ₂ O ₄ nanoparticles combined with UV-A light dramatically suppressed the growth of multiple bacteria in simulated wastewater within 30–60 min. While these NPs have inherent antimicrobial activity, surface functionalization or metal doping can greatly enhance their efficacy.	[31]
Ag-doped CoFe ₂ O ₄ NPs	Silver-doped NPs showed markedly higher antimicrobial activity than plain CoFe ₂ O ₄ NPs.	[32]
Cobalt–zinc ferrites	Removal of Pb ²⁺ from water and magnetic hyperthermal therapy	[33]
Cobalt ferrite–silica	Adsorbent for the malachite green removal from water	[34]
CoFe ₂ O ₄ /TiO ₂ nanocomposite	Photocatalytic activity	[35]

by the ROS activity (Figure 3), where higher concentrations yield greater antibacterial impact; however, cytotoxicity to mammalian cells is substantial at comparable doses (VERO and WI-38: 92.4% and 90.2% inhibition at 1000 µg·mL⁻¹, decreasing to 12.9% and 9.6% at 125 µg·mL⁻¹, Table 2), indicating a very significant therapeutic window as MICs didn't overlap with concentrations that produce notable host cell toxicity.

4. Conclusions

The study synthesized NiCdFe₂O₄ for medical applications using a co-precipitate method. The nanoparticles were found to be spherical with a crystallite size of less than 25 nm. The structural and magnetic properties were examined using FTIR and XRD. The nanoparticles demonstrated strong quantum confinement effects and superparamagnetic behavior at room temperature. The study tested NiCdFe₂O₄ nanoparticles against six multidrug-resistant and two ATCC bacterial strains, with *K. pneumoniae* being the most resistant. The nanoparticles effectively trapped bacterial infections by binding to areas on the *K. pneumoniae* surface, damaging the membrane's structural integrity. The efficiency of capture increased dramatically when the infection duration increased from 40 to 120 min.

CRedit authorship contribution statement

S.H.A : Formal analysis, Methodology, Writing – review & editing.

Declaration of competing interest

The authors declare no competing interests.

Data availability

The data will be available upon reasonable request from the corresponding author

Declaration of generative AI and AI-assisted technologies in the writing process

The author confirms that there was no use of artificial intelligence (AI)-assisted technology for assisting in the writing or editing of the manuscript and no images were manipulated using AI.

Acknowledgment

I sincerely appreciate Taibah University for its support in helping complete this research.

References

- Murray, C.J.L., Ikuta, K.S., Sharara, F., Swetschinski, L., Robles Aguilar, G., Gray, A., Han, C., Bisignano, C., Rao, P., Wool, E., Johnson, S.C., Browne, A.J., Chipeta, M.G., Fell, F., Hackett, S., Haines-Woodhouse, G., Kashef Hamadani, B.H., Kumaran, E.A.P., McManigal, B., Naghavi, M., 2022. Global burden of bacterial antimicrobial resistance in 2019: A systematic analysis. *The Lancet*, **399**, 629–655. [https://doi.org/10.1016/S0140-6736\(21\)02724-0](https://doi.org/10.1016/S0140-6736(21)02724-0)
- World Health Organization. (2020). *Antimicrobial resistance*. <https://www.who.int/news-room/fact-sheets/detail/antimicrobial-resistance>
- Dai, Y., Guo, Y., Tang, W., Chen, D., Xue, L., Chen, Y., Guo, Y., Wei, S., Wu, M., Dai, J., Wang, S., 2024. Reactive oxygen species-scavenging nanomaterials for the prevention and treatment of age-related diseases. *Journal of Nanobiotechnology*, **22**, 252. <https://doi.org/10.1186/s12951-024-02501-9>
- Topol, E.J., 2019. High-performance medicine: The convergence of human and artificial intelligence. *Nature Medicine*, **25**, 44–56. <https://doi.org/10.1038/s41591-018-0300-7>
- Fahim, Y.A., Hasani, I.W., Mahmoud Ragab, W., 2025. Promising biomedical applications using superparamagnetic nanoparticles. *European Journal of Medical Research*, **30**, 441. <https://doi.org/10.1186/s40001-025-02696-z>
- Ba-Abbad, M.M., Benamour, A., Ewis, D., Mohammad, A.W., Mahmoudi, E., 2022. Synthesis of Fe₃O₄ nanoparticles with different shapes through a co-precipitation method and their application. *Journal of The Minerals, Metals & Materials Society (TMS)*, **74**, 3531–3539. <https://doi.org/10.1007/s11837-022-05380-3>
- Ao, W., Wen, Z., Liu, L., Liu, P., Gan, Y., Wang, L., Li, L.K.B., 2022. Controlling the combustion and agglomeration characteristics of a solid composite propellant via a DC electric field. *Aerospace Science and Technology*, **128**, 107766. <https://doi.org/10.1016/j.ast.2022.107766>
- Mehrabi, F., Shamspur, T., Sheibani, H., Mostafavi, A., Mohamadi, M., Hakimi, H., Bahramabadi, R., Salari, E., 2021. Silver-coated magnetic nanoparticles as an efficient delivery system for the antibiotics trimethoprim and sulfamethoxazole against *E. Coli* and *S. aureus*: Release kinetics and antimicrobial activity. *Biometals : An International Journal on the Role of Metal Ions in Biology, Biochemistry, and Medicine*, **34**, 1237–1246. <https://doi.org/10.1007/s10534-021-00338-5>
- de la Fuente-Nunez, C., Cesaro, A., Hancock, R.E.W., 2023. Antibiotic failure: Beyond antimicrobial resistance. *Drug resistance updates : Reviews and Commentaries in*

- Antimicrobial and Anticancer Chemotherapy*, **71**, 101012. <https://doi.org/10.1016/j.drug.2023.101012>
- Li, F., Huang, T., Pasic, P., Easton, C.D., Voelcker, N.H., Heath, D.E., O'Brien-Simpson, N.M., O'Connor, A.J., Thissen, H., 2023. One step antimicrobial coatings for medical device applications based on low fouling polymers containing selenium nanoparticles. *Chemical Engineering Journal*, **467**, 143546. <https://doi.org/10.1016/j.cej.2023.143546>
 - Chaurasia, A.K., Thorat, N.D., Tandon, A., Kim, J.H., Park, S.H., Kim, K.K., 2016. Coupling of radiofrequency with magnetic nanoparticles treatment as an alternative physical antibacterial strategy against multiple drug resistant bacteria. *Scientific Reports*, **6**, 33662. <https://doi.org/10.1038/srep33662>
 - Shamaila, S., Zafar, N., Riaz, S., Sharif, R., Nazir, J., Naseem, S., 2016. Gold nanoparticles: An efficient antimicrobial agent against enteric bacterial human pathogen. *Nanomaterials (Basel, Switzerland)*, **6**, 71. <https://doi.org/10.3390/nano6040071>
 - Singh, S., Barick, K.C., Bahadur, D., 2011. Surface engineered magnetic nanoparticles for removal of toxic metal ions and bacterial pathogens. *Journal of Hazardous Materials*, **192**, 1539-1547. <https://doi.org/10.1016/j.jhazmat.2011.06.074>
 - Elwakil, B.H., Eldrieny, A.M., Almotairy, A.R.Z., El-Khatib, M., 2024. Potent biological activity of newly fabricated silver nanoparticles coated by a carbon shell synthesized by electrical arc. *Scientific Reports*, **14**, 5324. <https://doi.org/10.1038/s41598-024-54648-y>
 - Darabdhara, G., Boruah, P.K., Hussain, N., Borthakur, P., Sharma, B., Sengupta, P., Das, M.R., 2017. Magnetic nanoparticles towards efficient adsorption of gram positive and gram negative bacteria: An investigation of adsorption parameters and interaction mechanism. *Colloids and Surfaces A: Physicochemical and Engineering Aspects*, **516**, 161-170. <https://doi.org/10.1016/j.colsurfa.2016.12.003>
 - DuBois, M., Gilles, K.A., Hamilton, J.K., Rebers, P.A., Smith, F., 1956. Colorimetric method for determination of sugars and related substances. *Analytical Chemistry*, **28**, 350-356. <https://doi.org/10.1021/ac60111a017>
 - Bradford, M.M., 1976. A rapid and sensitive method for the quantitation of microgram quantities of protein utilizing the principle of protein-dye binding. *Analytical Biochemistry*, **72**, 248-254. [https://doi.org/10.1016/0003-2697\(76\)90527-3](https://doi.org/10.1016/0003-2697(76)90527-3)
 - Abdel Ghany, T.M., Ganash, M., Alawlaqi, M.M., Al-Rajhi, A.M.H., 2019. Antioxidant, antitumor, antimicrobial activities evaluation of *Musa paradisiaca* L. Pseudostem exudate cultivated in Saudi Arabia. *BioNanoScience*, **9**, 172-178. <https://doi.org/10.1007/s12668-018-0580-x>
 - Beal, J., Farny, N.G., Haddock-Angelli, T., Selvarajah, V., Baldwin, G.S., Buckley-Taylor, R., Gershater, M., Kiga, D., Marken, J., Sanchania, V., Sison, A., Workman, C.T., 2020. Robust estimation of bacterial cell count from optical density. *Communications Biology*, **3**, 512. <https://doi.org/10.1038/s42003-020-01127-5>
 - Kapur, M.A., Devi, M.K., Janani, R., Prasanna, J., Arumugam, N., Djearamane, S., Shing Wong, L., Kayarohanam, S., 2024. Simple biotic; spinel CoFe₂O₄ nanosphere for textile pollutant removal by photoresponsivity process and anti-microbial analysis. *Journal of King Saud University - Science*, **36**, 103369. <https://doi.org/10.1016/j.jksus.2024.103369>
 - Al-Humaidi, J.Y., Hagar, M., Bakr, B.A., Elwakil, B.H., Moneer, E.A., El-Khatib, M., 2022. Decorative multi-walled carbon nanotubes by ZnO: Synthesis, characterization, and potent anti-toxoplasmosis activity. *Metals*, **12**, 1246. <https://doi.org/10.3390/met12081246>
 - Toderaş, M., Aljohani, F.S., El-Khatib, M., 2024. Impact of electrical current on cluster nucleation production: Phase, structure, and nanosize for Al₂O₃. *Journal of Crystal Growth*, **625**, 127437. <https://doi.org/10.1016/j.jcrysgro.2023.127437>
 - Abd El-Moneim, A., Azooz, M.A., Hashem, H.A., Fayad, A.M., Elwan, R.L., 2023. XRD, FTIR and ultrasonic investigations of cadmium lead bismuthate glasses. *Scientific Reports*, **13**, 12788. <https://doi.org/10.1038/s41598-023-39489-5>
 - Rahman, M., Lutfur Rahman, M., Biswas, B., Farid Ahmed, M., Aftab Ali Shaikh, M., Akter Jahan, S., Sharmin, N., 2023. Effect of Ni-doping on coloring and photocatalytic performance of MgTi₂O₅ nanoceramics. *Journal of Industrial and Engineering Chemistry*, **126**, 340-359. <https://doi.org/10.1016/j.jiec.2023.06.024>
 - Lee, C., Kim, J.Y., Lee, W.I., Nelson, K.L., Yoon, J., Sedlak, D.L., 2008. Bactericidal effect of zero-valent iron nanoparticles on *Escherichia coli*. *Environmental Science & Technology*, **42**, 4927-4933. <https://doi.org/10.1021/es800408u>
 - Bromberg, L., Chang, E.P., Alvarez-Lorenzo, C., Magariños, B., Concheiro, A., Hatton, T.A., 2010. Binding of functionalized paramagnetic nanoparticles to bacterial lipopolysaccharides and DNA. *Langmuir: The ACS Journal of Surfaces and Colloids*, **26**, 8829-8835. <https://doi.org/10.1021/la904589p>
 - Gu, H., Xu, K., Xu, C., Xu, B., 2006. Biofunctional magnetic nanoparticles for protein separation and pathogen detection. *Chemical Communications (Cambridge, England)*, 941-949. <https://doi.org/10.1039/b514130c>
 - Tran, N., Mir, A., Mallik, D., Sinha, A., Nayar, S., Webster, T.J., 2010. Bactericidal effect of iron oxide nanoparticles on *Staphylococcus aureus*. *International Journal of Nanomedicine*, **5**, 277-283. <https://doi.org/10.2147/ijn.s9220>
 - Kooti, M., Saiahi, S., Motamedi, H., 2013. Fabrication of silver-coated cobalt ferrite nanocomposite and the study of its antibacterial activity. *Journal of Magnetism and Magnetic Materials*, **333**, 138-143. <https://doi.org/10.1016/j.jmmm.2012.12.038>
 - Madhukara Naik, M., Bhojya Naik, H.S., Nagaraju, G., Vinuth, M., Vinu, K., Viswanath, R., 2019. Green synthesis of zinc doped cobalt ferrite nanoparticles: Structural, optical, photocatalytic and antibacterial studies. *Nano-Structures & Nano-Objects*, **19**, 100322. <https://doi.org/10.1016/j.nanoso.2019.100322>
 - Rodríguez-Chueca, J., Barahona-García, E., Blanco-Gutiérrez, V., Isidoro-García, L., Dos santos-García, A.J., 2020. Magnetic CoFe₂O₄ ferrite for peroxymonosulfate activation for disinfection of wastewater. *Chemical Engineering Journal*, **398**, 125606. <https://doi.org/10.1016/j.cej.2020.125606>
 - Satheeshkumar, M.K., Kumar, E.R., Srinivas, C., Suriyanarayanan, N., Deepty, M., Prajapat, C.L., Rao, T.V.C., Sastry, D.L., 2019. Study of structural, morphological and magnetic properties of Ag substituted cobalt ferrite nanoparticles prepared by honey assisted combustion method and evaluation of their antibacterial activity. *Journal of Magnetism and Magnetic Materials*, **469**, 691-697. <https://doi.org/10.1016/j.jmmm.2018.09.039>
 - Tatarchuk, T., Shyichuk, A., Sojka, Z., Gryboś, J., Naushad, M., Kotsyubynsky, V., Kowalska, M., Kwiatkowska-Marks, S., Danyliuk, N., 2021. Green synthesis, structure, cations distribution and bonding characteristics of superparamagnetic cobalt-zinc ferrites nanoparticles for Pb(II) adsorption and magnetic hyperthermia applications. *Journal of Molecular Liquids*, **328**, 115375. <https://doi.org/10.1016/j.molliq.2021.115375>
 - Amiri, M., Salavati-Niasari, M., Akbari, A., Gholami, T., 2017. Removal of malachite green (a toxic dye) from water by cobalt ferrite silica magnetic nanocomposite: Herbal and green sol-gel autocombustion synthesis. *International Journal of Hydrogen Energy*, **42**, 24846-24860. <https://doi.org/10.1016/j.ijhydene.2017.08.077>
 - Puspitarum, D.L., Istiqomah, N.I., Tumbelaka, R.M., Kusumaatmaja, A., Oshima, D., Kato, T., Suharyadi, E., 2022. High performance of magnetically separable and recyclable photocatalyst of green-synthesized CoFe₂O₄/TiO₂ nanocomposites for degradation of methylene blue. *Advances in Natural Sciences: Nanoscience and Nanotechnology*, **13**, 045003. <https://doi.org/10.1088/2043-6262/ac996b>